PAPER

Tunas as a high-performance fish platform for inspiring the next generation of autonomous underwater vehicles

To cite this article: Dylan K Wainwright and George V Lauder 2020 Bioinspir. Biomim. 15 035007

View the article online for updates and enhancements.

Recent citations

- Tuna locomotion: a computational hydrodynamic analysis of finlet function Junshi Wang et al



IOP ebooks™

Bringing together innovative digital publishing with leading authors from the global scientific community.

Start exploring the collection-download the first chapter of every title for free.

Bioinspiration & Biomimetics



RECEIVED 19 November 2019

REVISED
29 January 2020

ACCEPTED FOR PURI ICATIO

ACCEPTED FOR PUBLICATION 13 February 2020

PUBLISHED 25 March 2020

PAPER

Tunas as a high-performance fish platform for inspiring the next generation of autonomous underwater vehicles

Dylan K Wainwright 1,2,3 10 and George V Lauder 1 10

- ¹ Harvard University, Museum of Comparative Zoology, 26 Oxford Street, Cambridge MA 02143, United States of America
- ² Yale University, Peabody Museum of Natural History, 21 Sachem Street, New Haven CT 06511, United States of America
- ³ Author to whom any correspondence should be addressed.

E-mail: dylan.wainwright@yale.edu and dylan.wainwright@gmail.com

Keywords: locomotion, robotics, finlets, keels, pectoral fin, morphology

Supplementary material for this article is available online

Abstract

Tunas of the genus *Thunnus* are a group of high-performance pelagic fishes with many locomotor traits that are convergently shared with other high-performance fish groups. Because of their swimming abilities, tunas continue to be an inspiration for both comparative biomechanics and the design of biomimetic autonomous underwater vehicles (AUVs). Despite the strong history of studies in tuna physiology and current interest in tuna biomechanics and bio-inspired design, we lack quantitative data on the function of many features of tunas. Here we present data on the morphology, behavior, and function of tunas, focusing especially on experimentally examining the function of tuna lateral keels, finlets, and pectoral fins by using simple physical models. We find that both triangular lateral keels and flexible finlets decrease power requirements during swimming, likely by reducing lateral forces and yaw torques (compared to models either without keels or with rectangular keels, and models with stiff finlets or strip fins of equal area, respectively). However, both triangular keels and flexible finlets generate less thrust than other models either without these features or with modified keels or finlets, leading to a tradeoff between power consumption and thrust. In addition, we use micro computed tomography (μ CT) to show that the flexible lateral keels possess a lateral line canal, suggesting these keels have a sensory function. The curved and fully-attached base of tuna pectoral fins provides high lift-to-drag ratio at low angles of attack, and generates the highest torques across speeds and angles of attack. Therefore, curved, fully-attached pectoral fins grant both better gliding and maneuvering performance compared to flat or curved, partially-attached designs. We provide both 3D models of tuna morphology derived from μ CT scans and conclusions about the performance effects of tuna-like features as a resource for future biological and engineering work for next-generation tuna-inspired AUV designs.

1. Introduction

The design of biomimetic autonomous underwater vehicles (AUVs) is a rapidly expanding area of research, in large part due to the growing availability of manufacturing methods like additive manufacturing (e.g. 3D printing) and the increasingly integrative nature of engineering and biology. However, the design of biomimetic AUVs is far from a mature field, and most bio-inspired AUV designs are only loosely based on the shape and general kinematics of a swimming animal [1–3]. In many cases, we lack a mechanistic

understanding of the functional morphology of swimming animals and therefore cannot prescribe particular biomimetic design features for AUVs and expect a specific subsequent change in capability or performance. In fact, because of this lack of biomechanical knowledge, AUVs and other robotic platforms are often used instead to inspire or test biological questions about the function of organisms in the developing area of robotics-inspired biology [4, 5]. In this paper we aim to connect bio-inspired AUV design to organismal biomechanics by testing the function and performance of three features of high-

performance fishes and presenting an overview of high-performance fish functional design as a basis for future fish-inspired AUV design.

An archetypal group of large-bodied, high-performance fishes that have continued to provide inspiration for AUV designs are the tunas (Thunnus species, family Scombridae). Tunas in the genus Thunnus regularly migrate long distances across ocean basins [6, 7] and they have a number of adaptations related to increased swimming performance, including streamlined bodies, increased aerobic scope, and a regionally-endothermic physiology (tunas maintain elevated temperatures in the core of their body) [8]. Tunas have many features that are convergently shared (evolved independently and not shared because of genetic relatedness) with other groups of pelagic, highperformance fishes, leading researchers to surmise that these features may increase swimming performance. However, the lack of data-driven approaches to investigate the performance of these features has generated a number of hypotheses about tuna functional morphology, but scarce quantitative study. The gap in knowledge regarding the function of tuna locomotor traits is especially concerning considering that tunas are an excellent model for high performance swimming and thus remain an important group for the design of high-performance, bio-inspired AUV platforms [9–14].

Our descriptions of tuna functional morphology integrate 3D morphological observations from micro computed tomography (μ CT) scanning with investigations of behavior, resulting in the testing of physical models to explore the function of three locomotor features of tunas. We limit our morphological descriptions to observations that we believe are relevant to tunas as both high-performance swimmers and AUV platforms, as there are a number of detailed descriptions of tuna anatomy already in the biological literature [15-21]. In particular, we emphasize the 3D conformation of locomotor anatomy by using threedimensional (3D) and cross-sectional views from μ CT and histology. To support future work on tuna morphology and bioinspired design, we also include .stl files generated from our μ CT scans (see supplementary material (stacks.iop.org/BB/15/035007/mmedia)).

In this paper, we first briefly provide an overview of body and tail morphology in tunas (figures 1 and 2). Second, we present data on the structure and function of lateral keels, finlets, and pectoral fins using morphology (figures 3–5), behavior (figure 6) and experiments on physical models of these three features (figures 7–10). For the keel experiments we address the influence of lateral peduncle keels on swimming performance. Lateral peduncle keels are fleshy lateral projections of tissue that occur at the narrowest part of the caudal peduncle as the body narrows to attach to the caudal fin (figure 3). Lateral keels have convergently evolved in other species besides tunas and their relatives (Scombridae), as similar structures also occur in

swordfish (*Xiphias gladius*), Carangidae (jacks), Lamnidae (mako, white, porbeagle, and salmon sharks), whale sharks (*Rhincodon typus*), and some cetaceans (dolphins and whales). These animals are all large, high-performance swimmers that constantly swim and can undertake substantial migrations, suggesting that peduncle keels are relevant to a perpetually-swimming pelagic lifestyle.

Finlets are small, triangular fins that line the dorsal and ventral edge of tunas between the second dorsal fin and the caudal fin (figure 4), and they have convergently evolved in other high-performance fishes, including species within Carangidae (jacks), Scomberosocidae (sauries), and both extinct and extant species in the Clupeidae (anchovies). In addition, the second dorsal fins of many sharks and billfishes (Istiophoriformes) have a similar appearance to finlets. Finlets are independently controllable through three pairs of muscles that attach to the leading-edge base of each finlet [22]. However, the normal pattern of movement for finlets has been suggested to be passive because during steady swimming, finlets oscillate from side-toside about their base as expected based on fluid flow at their location ([22], figure 6). In tunas, species have anywhere from 6-10 finlets on each of their dorsal and ventral edges [20], and in mackerel, total finlet area sums to 15% of the area of the caudal fin and finlets are larger posteriorly [22]. Although finlet morphology and function have been studied more than keel mechanics [22, 23], we still do not understand how finlets are changing swimming performance and theories abound concerning finlet function. Previous researchers have suggested that finlets might contribute to thrust by directing flow towards the middle of the caudal fin [22], decrease drag by directing flow longitudinally [18, 22], increase lift produced by lateral keels [24], or dampen turbulence and cross flow across the dorsal and ventral edges of the body [25–27]. We used passively flexible models of finlets to assess how these structures affect swimming performance.

Finally, we investigated the performance effects of tuna pectoral fin design. Pectoral fins are a set of paired fins common to nearly all fishes that are often located just posterior to the gill opening on the right and left sides of the body (figure 5). In most fishes, pectoral fins are used for maneuvering or thrust production [28,29], but in tunas they have been substantially stiffened and elongated to appear as long, swept airfoils. Tunas deploy their pectoral fins laterally from the sides of their body (figure 6) and thereby generate lift forces during swimming, which are thought to help them maintain a stable horizontal swimming position at low speeds [19, 24]. Previous estimates of lift generated by tuna pectoral fins have assumed a flat conformation. However, we noticed that the base of the pectoral fin has a trailing edge that is curved ventrally in both tuna species we examined (figure 5), giving tuna pectoral fins a complex 3D conformation. Thus, we designed a set of simple physical models mimicking the shape of

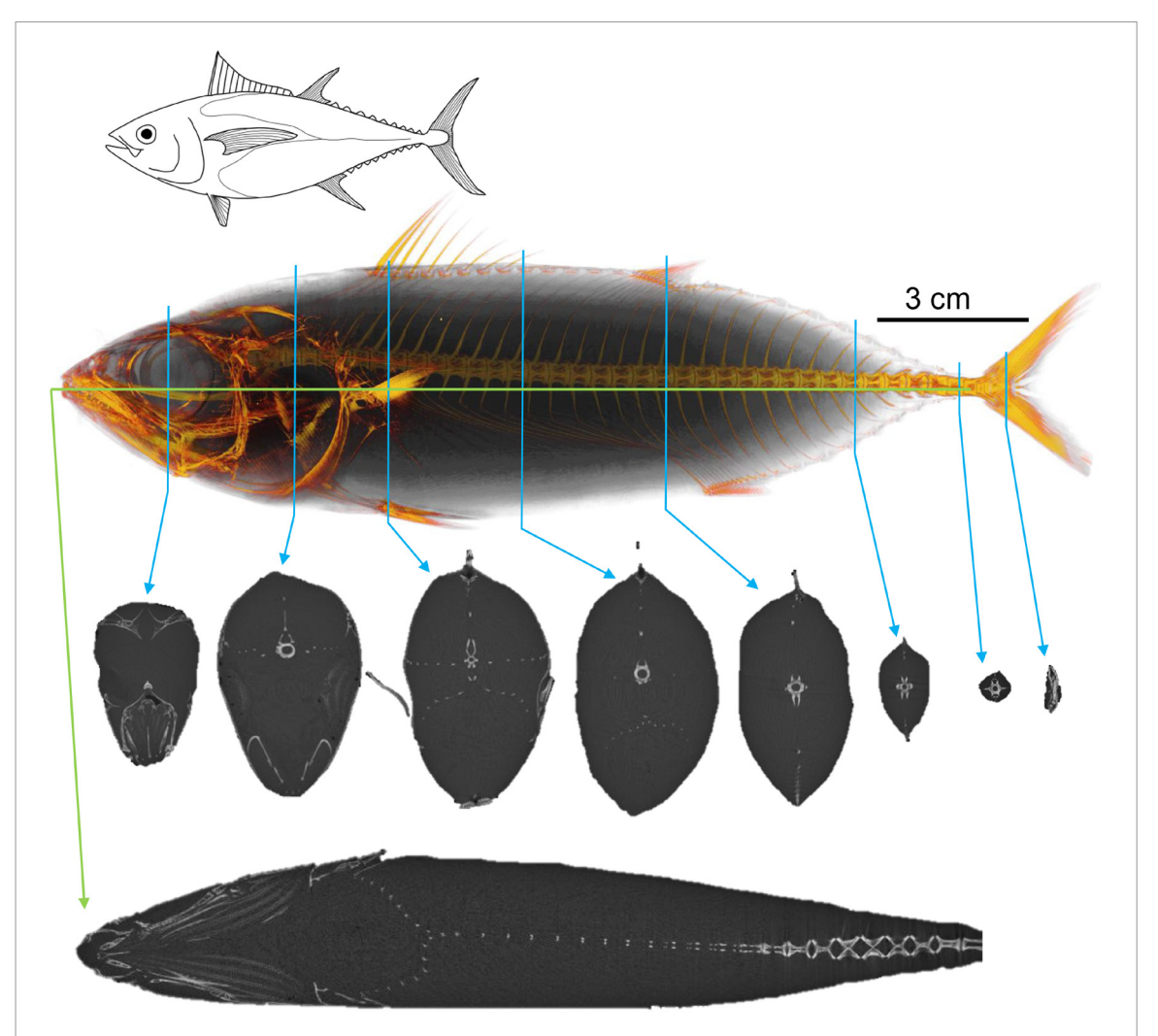


Figure 1. Gross morphology of the tuna body. Images are volume renders and slices from a μ CT scan of a small (fork length: 21 cm) Pacific bluefin tuna (*Thunnus orientalis*) with slices at different lengths along the body to show longitudinal variation in cross-sectional shape. Even this small individual shows the typical body shape of tunas—a streamlined and generally airfoil-shaped wide body narrowing to a small lunate caudal fin.

a Pacific bluefin tuna (*Thunnus orientalis*) pectoral fin to test how curvature and the attached base affect performance measured as the lift-to-drag ratio and torque generation.

2. Materials and methods

2.1. Tuna morphology

We primarily used micro-computed tomography (μ CT) to explore the morphology of tunas. Using this method, we scanned and imaged a small Pacific bluefin tuna (*Thunnus orientalis*; figure 1), the peduncle and caudal fin from an adult yellowfin tuna (*Thunnus albacares*; figure 2), the pectoral fins of both an adult yellowfin and adult Pacific bluefin tuna (figure 5), the peduncle and lateral keel of an adult yellowfin and an albacore tuna (*Thunnus alalunga*; figure 3), and the finlets from an adult yellowfin tuna (figure 4). Specimens of the peduncle and lateral keels in figure 3 were stained with a 2% weight-by-volume solution of iodine potassium iodide (IKI) to visualize soft tissues [30, 31], but otherwise specimens were scanned after being frozen and thawed (figures 1–3)

or after fixation in formalin and preservation in 70% ethanol (figure 4). For all μ CT scans, we used a Bruker Skyscan 1173 benchtop system (Bruker microCT, Kontich, Belgium) and performed scans ranging from 10–35 μ m resolution, 40–80 kV voltage, 116–200 μ A current, and 800–1200 ms of exposure. Scan parameters were tuned based on size of the specimen and higher voltages were used if the specimen was stained. We then reconstructed scan projections into slices using NRecon (Bruker microCT) and segmented morphology using Mimics v20 (Materialise, Leuven, Belgium). Volume rendering was done using CTvox v3.2 (Bruker micro CT).

For the lateral keels, we supplemented CT imaging with histological sections using both sirius red and haematoxylin and eosin stained sections of the lateral keel from a yellowfin tuna (thin sections of tissue are cut, stained to visualize tissue type, and mounted on slides for microscopy). Tissue was embedded in paraffin and sections were cut at a thickness of $10~\mu m$ in the transverse plane of the fish. We conducted additional investigation of gross morphology on both live and fresh-caught individuals of yellowfin tuna.

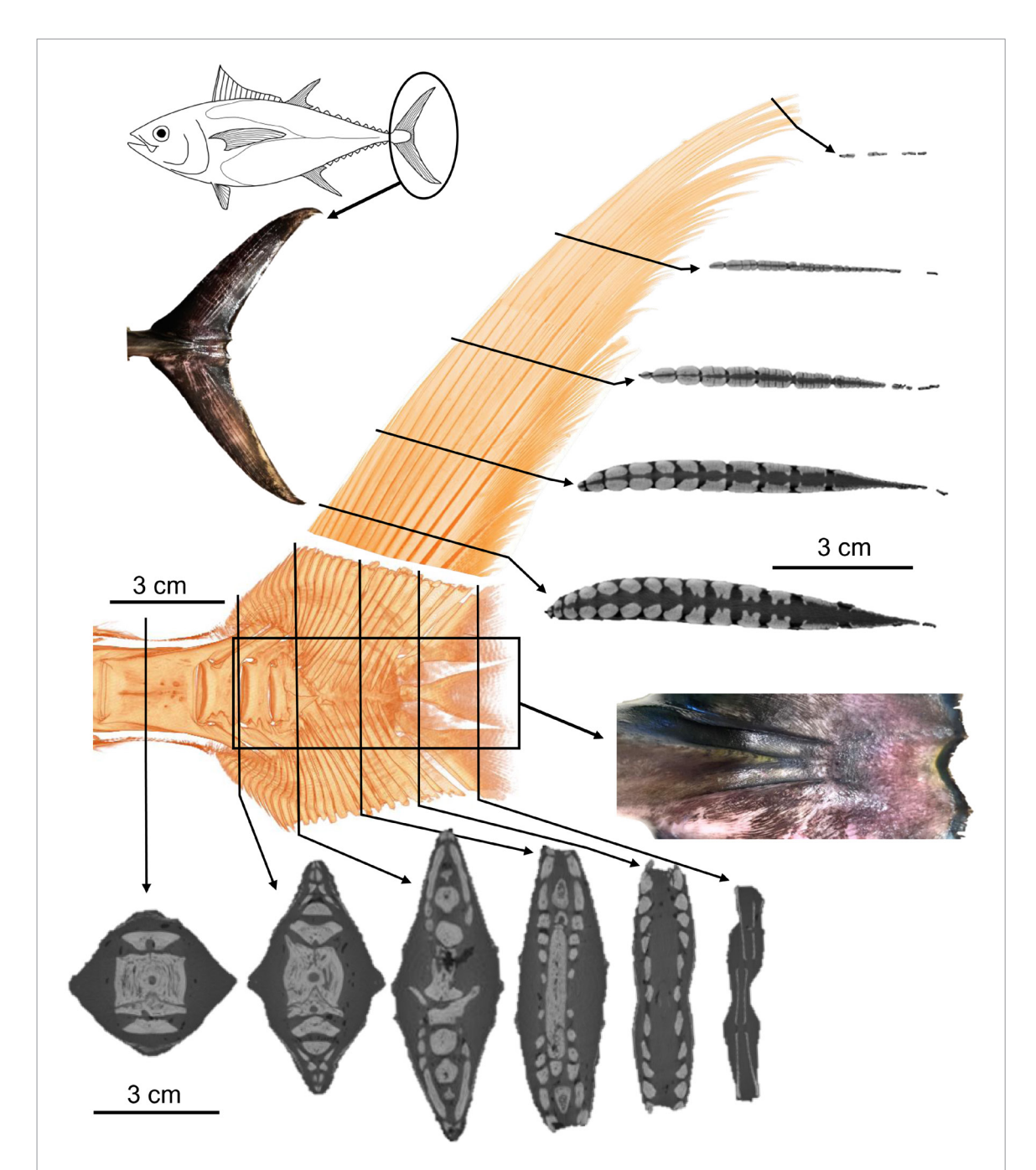


Figure 2. Caudal fin morphology of yellowfin tuna (*Thunnus albacares*) with a volume render of two μ CT scans shown in orange color. Slices show the cross-section at the end of the peduncle and the center of the caudal fin at bottom. Slices at right show the cross-section of the dorsal lobe of the caudal fin. Photograph inset at lower right shows the surface of the center of the caudal fin with small converging lateral keels along with the end of the lateral peduncle keel. Photograph also shows the notched trailing edge of the center of the caudal fin.

2.2. Tuna locomotor behavior

Live, wild-caught yellowfin tunas were studied at the Greenfins Aquaculture Tuna Center at University of Rhode Island's Bay Campus. Live yellowfin tunas (~1 m fork-length) were kept in a 40-foot diameter round tank holding approximately 125 000 gallons of seawater. We filmed tunas during routine swimming using both submerged GoPro Hero 5 cameras (GoPro Inc., USA) filming at 120 fps, and a submerged Photron Mini AX50 high-speed camera (Photron USA Inc., San Diego, CA, USA) filming at 500 fps. We also filmed tuna feeding bouts to capture high-speed maneuvers using the Photron Mini AX50 filming at 1000 fps.

2.3. Physical modeling and performance testing of lateral keels

We sought to study the function of the lateral keels of tunas to understand both their potential utility for AUV platforms and their biological function. To this end, we manufactured a tuna-like foil by laser cutting shim stock plastic sheeting (ARTUS Corp., Englewood, NJ, USA; coral color, thickness: 0.03 inches) in the shape seen in figure 7(a). This foil shape is a 2D representation of the posterior half of a tuna's body and it has a fork length of 18 cm (figure 7). We then added material (shim stock plastic sheeting cut into 5 cm by 8 cm, blue color, thickness: 0.005

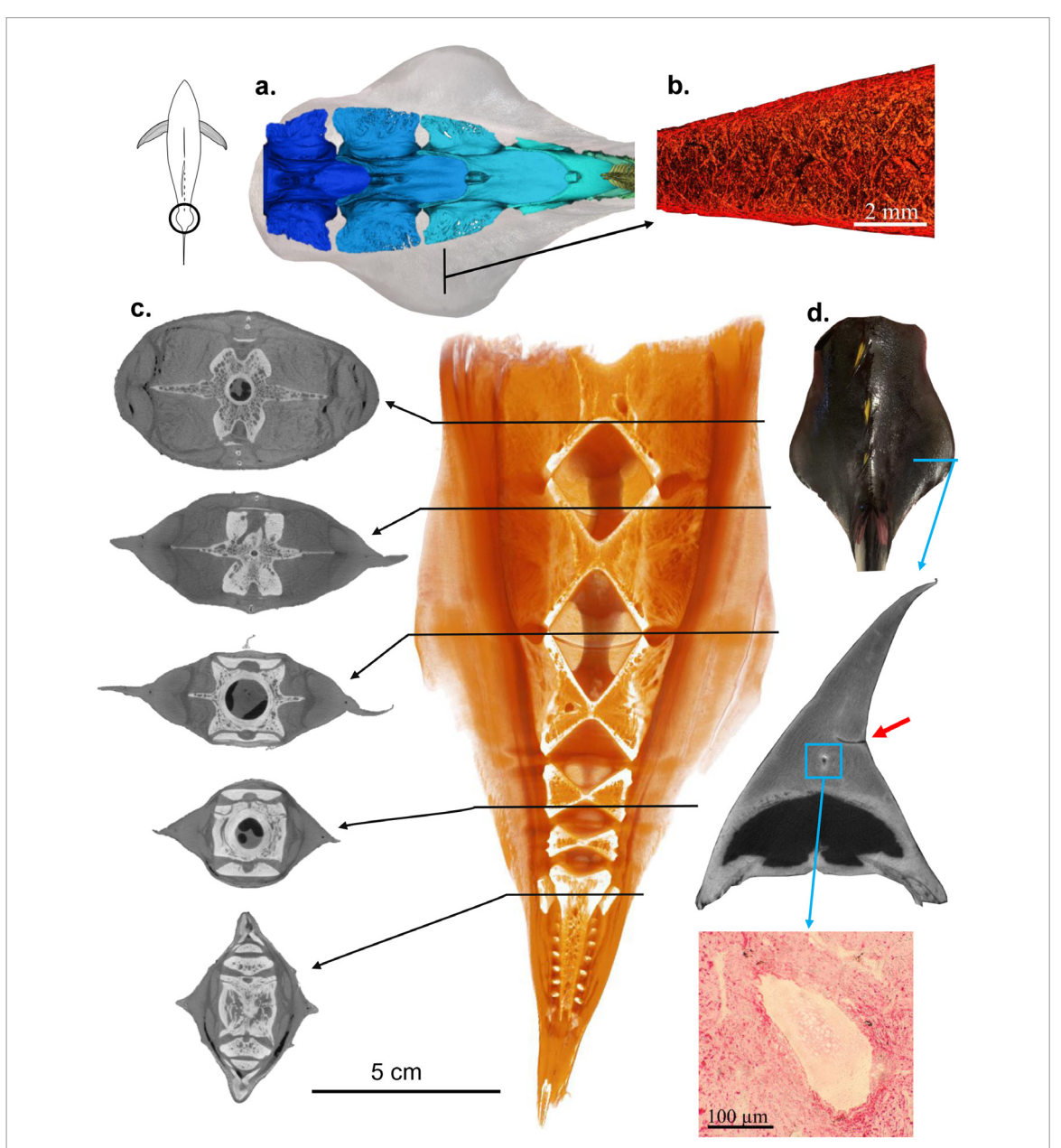


Figure 3. Lateral peduncle keels of tunas. (a) Dorsal view of a surface rendering of the bones of the caudal peduncle (albacore, *Thunnus alalunga*) overlayed with a photograph of a tuna peduncle, showing the offset position of the bony lateral keels and the fleshy lateral external keels. (b) Histological section of the lateral keel from region shown in 'a'. The keel is made largely of collagen (stained red). (c) Dorsal view of a volume render showing the interior morphology by digitally removing the upper half of peduncular tissue. Also shown at left are frontal views of cross sections from a contrast-stained μ CT scan of a yellowfin tuna (*Thunnus albacares*). Haemal and neural spines (dorsal and ventral bony processes that are flattened in tuna peduncles) are modified to overlap with the trailing vertebral centra, preventing dorso-ventral movement. (d) Cross section of a single lateral keel from a contrast-stained μ CT scan from a yellowfin tuna. Note the internal lateral line canal inside the blue box and the pore canal indicated by the red arrow. Histological section of the canal is given below, stained with hematoxylin and eosin.

inches) at the peduncle of these foils in different configurations to approximate lateral keels or the lack thereof. The peduncle material was folded into three different configurations: (1) flat against the peduncle, (2) a hollow, square cross-section keel, and (3) a hollow triangular-cross section keel, as seen in tunas (figures 3 and 7). The biomimetic, triangular keel design was manufactured to approximate the relative shape of a tuna keel, and the two keeled models were made with proportionally larger keels than tunas to increase our ability to detect differences among models. With the three foil designs (figure 7(a)), we tested how biomimetic lateral triangular keels change swimming

performance compared to models lacking keels or with square keels.

To compare the swimming performance of these three foils, we followed an experimental protocol similar to previous flapping-foil experiments conducted in the same experimental flow tank [32–34]. We mounted the foils on a rod attached to a six-axis force-torque transducer (ATI Inc., Apex North Carolina, USA) and then attached the rod and transducer onto a carriage that controlled pitch (rod rotation) and heave (lateral, or side-to-side) motion. The foil was then lowered into the working section of a recirculating flow tank and performance measured by

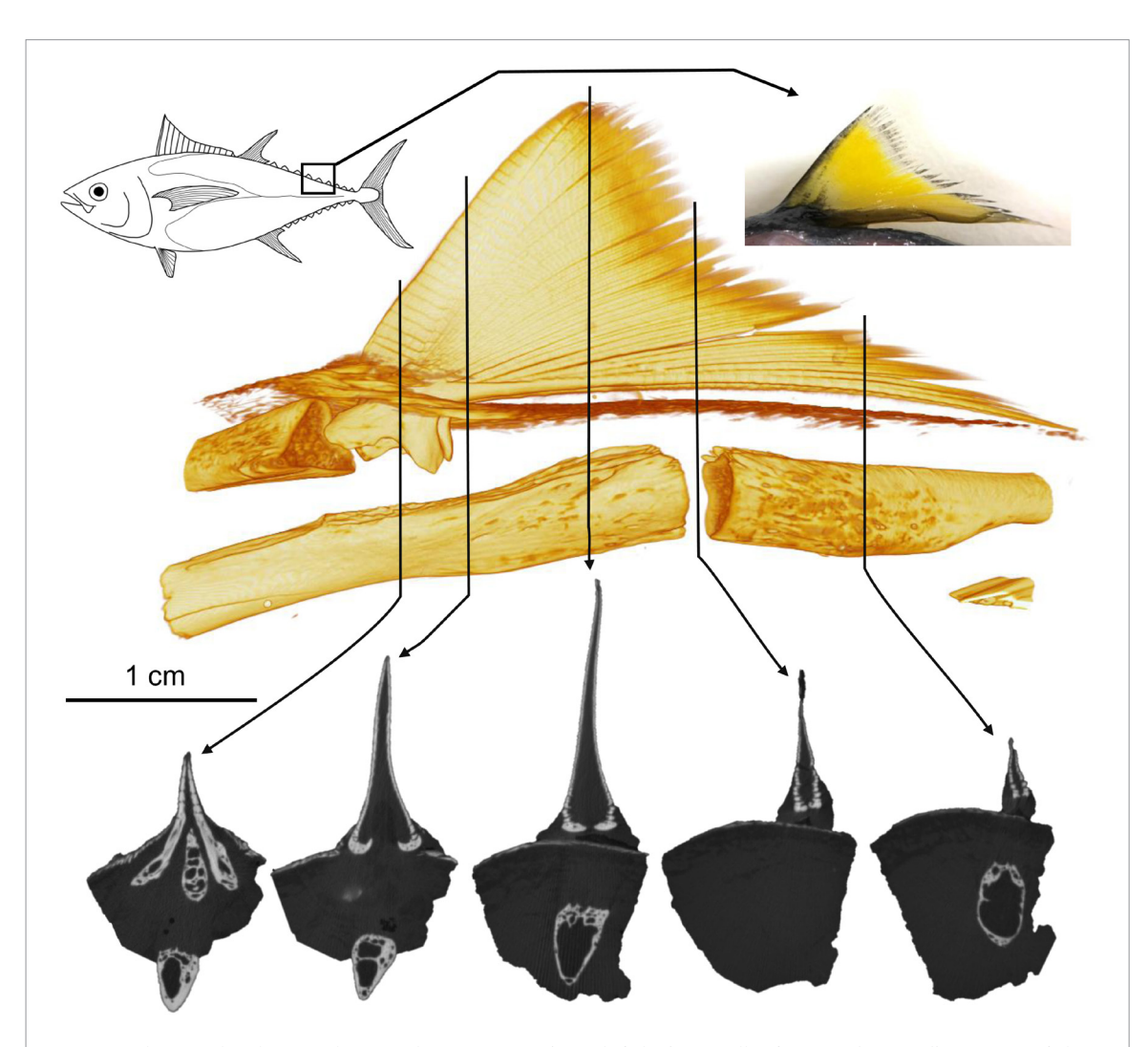


Figure 4. Photograph, volume rendering, and cross sections of a single finlet from a yellowfin tuna, *Thunnus albacares*. Tuna finlets are attached to the body anteriorly with both muscular and skeletal supports allowing active finlet movement but are otherwise separate from the body along their length. Bony supports are visible below the finlet embedded into the dorsal body region of tuna. Muscles extending from the skeletal supports to the base of the finlet are not shown (see supplementary movies). Bottom images show cross-sections from uCT finlet scans to illustrate the changing relationship between the external finlet and the interior skeletal supports.

flapping the foil using a prescribed motion program while recording force, torque, and power data from the transducer and the control motors. We moved all three foils in a sinusoidal manner using a leading-edge frequency of 2 Hz, ± 2 cm of heave motion, and 15° of pitch, offset by a 90° phase to better approximate tunalike midline kinematics as in our previous research [35]. All three foils were tested using this same motion program at three different velocities: 0.3 m s⁻¹, 0.46 m s^{-1} , and 0.6 m s^{-1} . These values were chosen because preliminary testing showed that 0.46 m s⁻¹ was near the self-propelled speed for these foils, so these flow speeds represent locomotor regimes of net thrust production (0.3 m s⁻¹), station holding (0.46 m s⁻¹: self-propelled speed), and net drag during swimming $(0.6 \,\mathrm{m\,s^{-1}})$ (also see [36]). We collected eight replicates of data for each foil at each speed. Each trial consisted of 10 s of data sampled at a rate of 1000 Hz.

In this experiment, our primary hypothesis was that lateral keels improve steady-swimming performance by reducing lateral forces generated by the peduncle, and thus increase locomotor efficiency by reducing side forces which do not contribute to thrust. To test this idea, we measured power, thrust, and all six directional forces and torques, with special interest in lateral forces and yaw torque (torque about the rod axis).

Data processing and statistics were performed in R v3.5.3 (R Foundation for statistical computing, Vienna, Austria). Forces in the lateral and thrust-drag axes were corrected to account for transducer rotation during the imposed motion program. Forces and torques were measured as the amplitude between the maximum and minimum values over five tail-beat cycles after raw data were filtered using a low-pass filter generated and applied using the butter() and filtfilt() commands from the signal package in R [37]. Analysis of variance (ANOVA) was used to compare how our three different foils performed across a number of measured performance variables. We then used TukeyHSD post hoc tests on significant ANOVA results to determine which foils performed differently given a flow speed and performance metric (force, torque, power, etc).

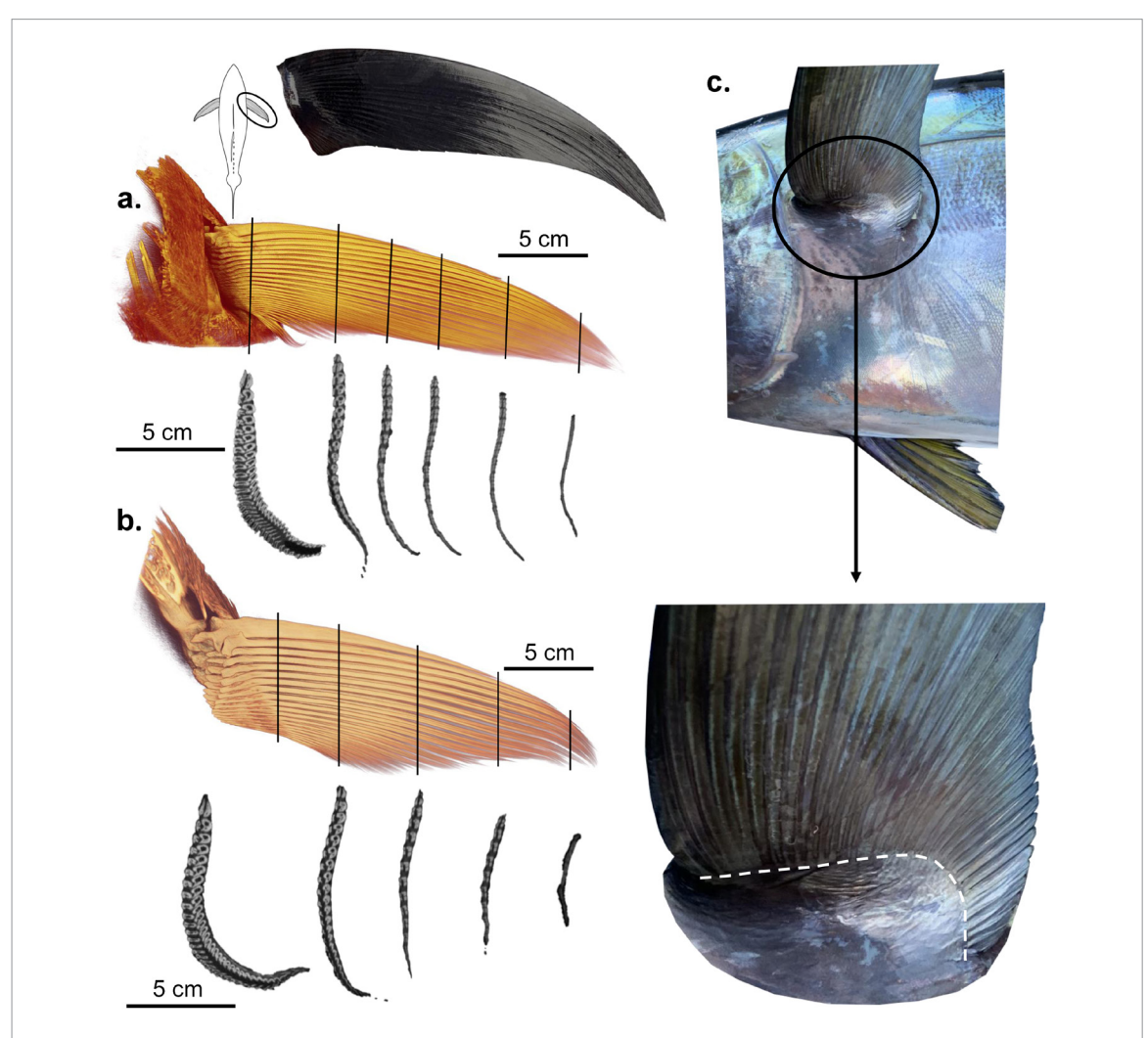


Figure 5. Tuna pectoral fins. (a) Pectoral fin of yellowfin tuna (*Thunnus albacares*) shown as a volume render from a μ CT scan and corresponding cross-sectional slices. Base of the pectoral fin is curved so that the trailing edge points ventrally. (b) Volume render of the pectoral fin of the Pacific bluefin tuna (*Thunnus orientalis*) with cross-sectional slices. Base of the pectoral is more curved than in yellowfin tuna. Ventral is to the right in slice images. (c) Photographs of a live yellowfin tuna showing the curved attachment of the base of the pectoral fin, outlined in dashed white line in image below.

2.4. Physical modeling and performance testing of finlets

We used processes similar to those outlined above in section 2.3 to study the effects of finlets on swimming performance. In this case, foils were made of one piece of thinner shim stock (color: green, thickness: 0.003 inches) cut in the shape of a tuna-like tail sandwiched between two pieces of thicker shim stock (color: black, thickness: 0.0125 inches). The thinner green shim stock was cut with three different finlet designs: (1) biomimetic finlets with cut bases, allowing for bending, (2) finlets with uncut bases that remain stiff, and (3) a long rectangular strip fin of equal area to the finlets that started from the same place as the first finlet on the other models and ended where the last finlets ended. The biomimetic flexible finlets were designed to be slightly larger than the relative area ratio between the caudal fin and finlets in adult tunas and mackerels (15%-20% in tunas and mackerels, 27% in our models) to improve our ability to detect differences among models. Using these three models, we were able to explore how the presence and design of finlets affects swimming performance. We used the same experimental setup,

testing platform, and motion program (2 Hz, 2 cm heave, 15° pitch, 90° phase delay) as in section 2.3. In contrast to the three speeds tested above, we tested the finlet model foils over eight replicates each at nine speeds: $0.35-0.75 \, \mathrm{m \, s^{-1}}$ at intervals of $0.05 \, \mathrm{m \, s^{-1}}$. Data were processed and analyzed similarly to the manner described above.

2.5. Physical modeling and performance testing of pectoral fins

We used shim stock (color: coral, thickness: 0.03 inches) models based on the pectoral fin of Pacific bluefin tuna to study how position and shape of the pectoral fin affects swimming performance and maneuverability under static conditions. Our models were all cut to the same shape (~8.5 cm from base to tip, which corresponds to pectoral fins from a fish 22 cm in fork length) and then bent into three different shapes. (1) A biomimetic model where the fin was heated and curved to match the curvature of a Pacific bluefin tuna and then was attached to the rod at both the leading and trailing edge. (2) A model where the pectoral fin model was curved to match that of tuna, but the model was

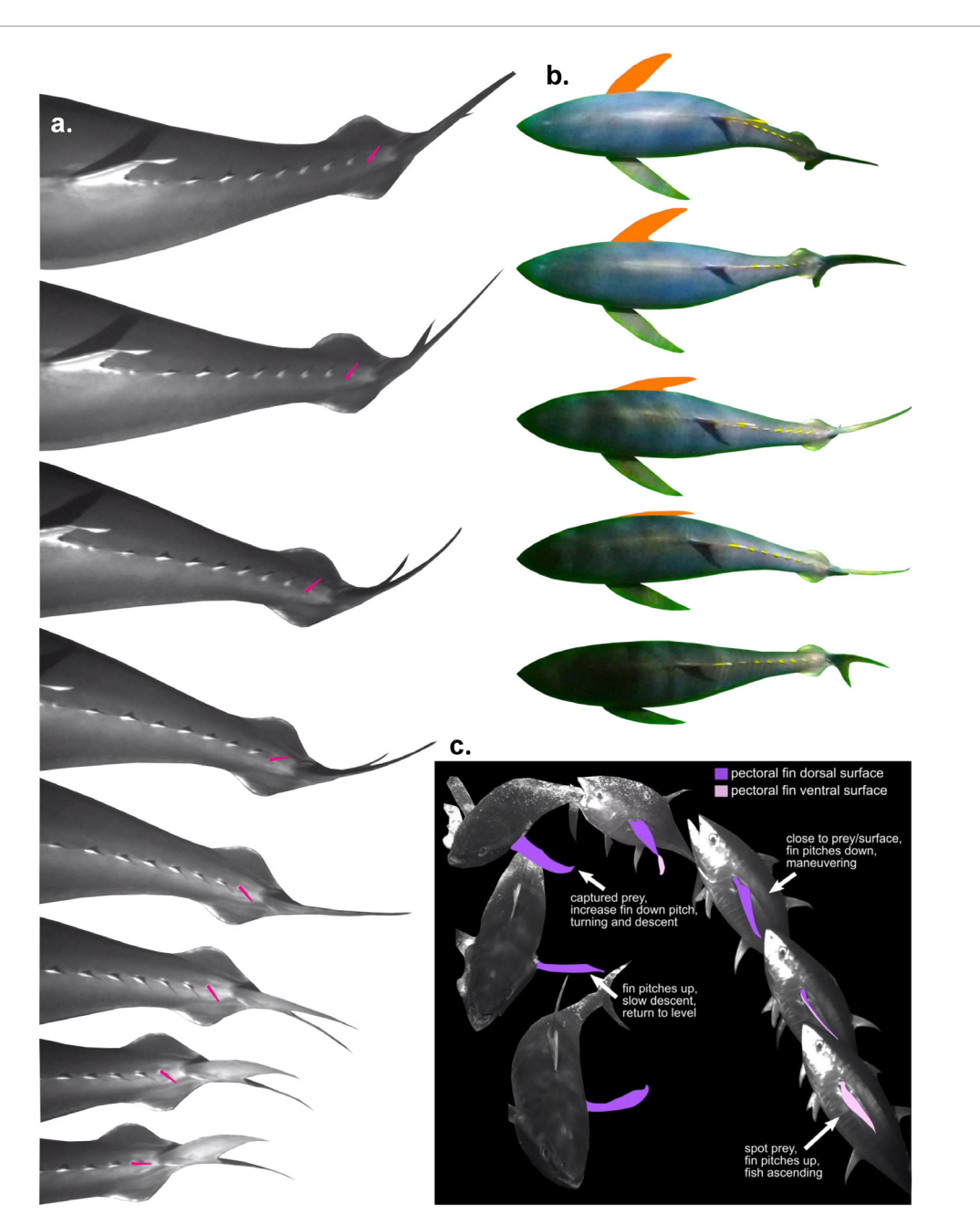


Figure 6. Kinematics of finlets and pectoral fins of yellowfin tuna, *Thunnus albacares*. (a) Finlet movement over one full tail beat is shown in dorsal view with the posterior-most finlet highlighted in red. This tuna is moving right to left in the image sequence, and swimming at approximately $1 \, \mathrm{m \, s^{-1}}$ or $1.0 \, \mathrm{l \, s^{-1}}$. More anterior finlets have lower oscillation amplitudes. (b) Pectoral fin position and deployment of a single pectoral fin from a dorsal view. Fin that folds against body is colored orange. After fin is folded, opposite side pectoral fin is still partially deployed during swimming. (c) Pectoral fin activity during a feeding event to illustrate a range of pectoral fin conformations. This sequence shows a single individual tuna approach a prey item from below, capture the prey near the surface, and descend and turn after prey capture. During this event, the pectoral fin makes large, active changes in its angle of attack during ascending, braking, descending, and then leveling out after descending. Dorsal surface of pectoral fin is colored purple and ventral surface is colored pink.

only attached to the rod at the leading edge, allowing a free trailing edge. (3) A model where the fin was flat with no curvature. We attached a single model to the rod in the same experimental setup as in section 2.3, to allow measurement of the torques produced by one fin. However in this case the model was attached so that the span of the pectoral fin was perpendicular to flow, as in live fish (figures 6 and 7). Along with the goal of investigating the effect of pectoral base curvature and attachment, testing of a single fin allowed us to evaluate relative forces and torques generated by the single-fin deployment behavior shown in figure 6.

In these experiments we did not move the fin model and instead recorded forces and torques under static conditions at two different flow speeds (0.22 and 0.44 m s⁻¹, corresponding to one and two body-lengths per second for the size of our model) and with the fins tilted at three different angles of attack (0°, 15°, and 30°; values above zero indicate that the leading edge is elevated) at each flow speed. Although these angles may at first seem high for seemingly immobile tuna pectoral fins, video sequences of high-speed maneuvering during feeding show that pectoral fins of tuna passively and actively perform at a wide range of angles

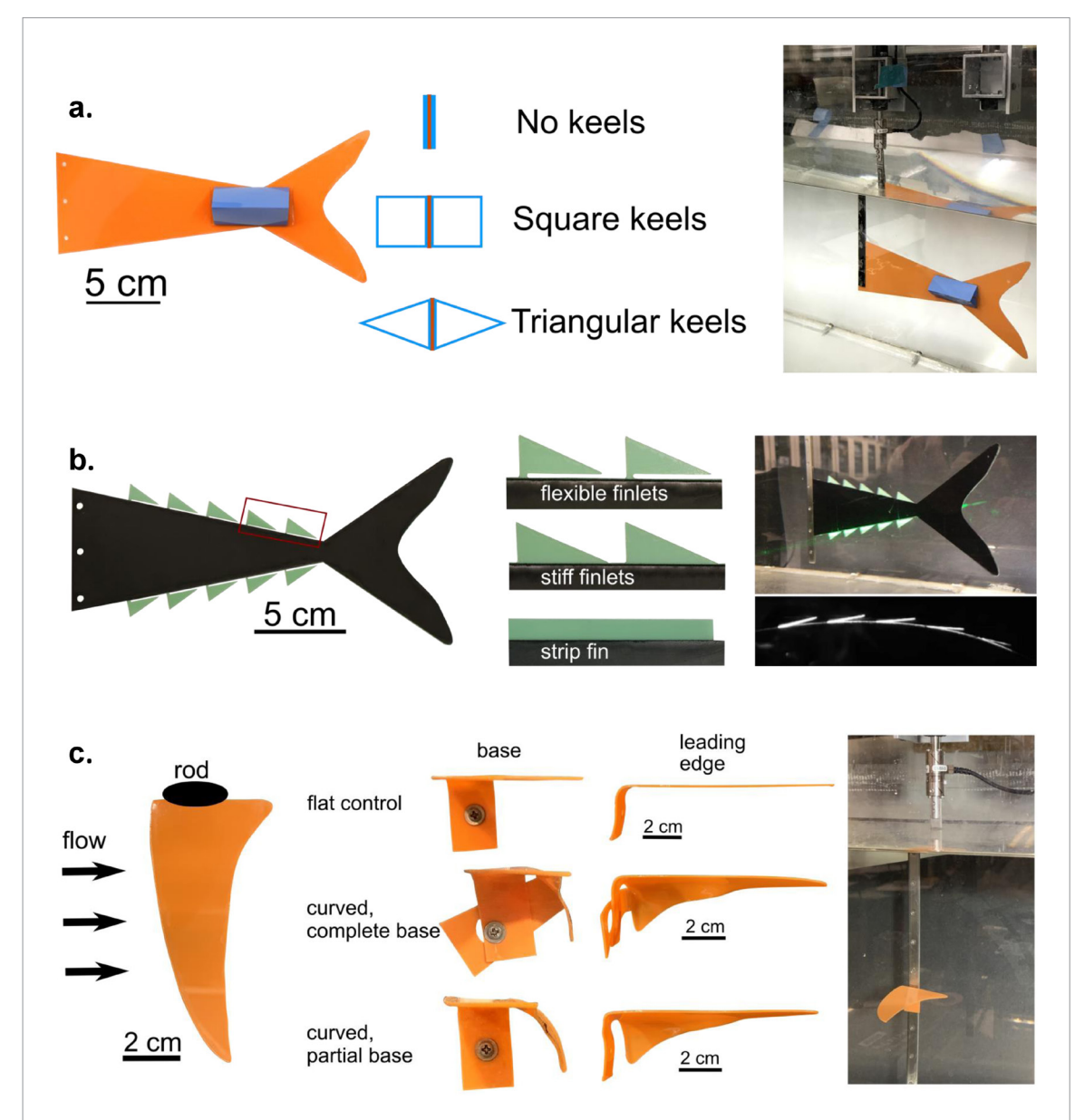


Figure 7. Physical model designs for three experiments testing the performance of different features of tunas. (a) Three models test how lateral keels change swimming performance: a model without keels but the same mass of material at the peduncle, a model with square cross-section keels, and a model with biomimetic triangular keels. All models were made with the same amount of material to keep mass consistent. Photograph at right shows the biomimetic keel model in the test section of a flow tank. (b) Three models test the function of finlets on swimming performance: a biomimetic model with passively flexible finlets (cut bases), a model with stiff finlets, and a model with dorsal and ventral strip fins that were the same area as the finlets. All models were made with the same amount of material to control for mass and surface area. Photographs at right show the model in a flow tank and a ventral view of the finlets during locomotion. The finlets are shown clearly bending away from the model midline. (c) Three models test the function of tuna pectoral fin shapes and the curved base: a flat model, a biomimetic curved model with a fully attached base, and a curved-base model with attachment just at the leading edge. Panel at right shows the testing setup with just a single model pectoral tested in flow; the ATI force/torque sensor is visible above the water.

(figure 6), and that tuna pectoral fins achieve angles of attack nearing 45° during some maneuvers. Data were then processed and analyzed as in section 2.3.

3. Results

3.1. Morphology of tunas

Tuna body shape has often been compared to similarly-shaped airfoils that have maximum thickness at around 50% of chord length [18]. Our results generally confirm this observation: tunas have thickened bodies with a very narrow caudal peduncular region, and

relatively small caudal fins surfaces for their body mass (figure 1).

Tuna caudal fins are rigid compared to most other fishes, and μ CT scans demonstrate the robust nature of the paired fin rays that make up dorsal and ventral lobes of the caudal fin (figure 2). Cross sections of the dorsal caudal fin lobe show an airfoil-like profile. Cross sections of the posterior end of the caudal peduncle and the center of the caudal fin show the overlapping nature of the most posterior vertebrae and the morphology of the uroneural and hypural bones (axial bones at the base of the caudal fin) that support the fin rays.

The fleshy lateral keels end at the center of the caudal fin and the skin near the posterior end of the fleshy keel also has two smaller keel-like ridges—one dorsal and one ventral to the centrally located fleshy keel (figure 2). The trailing edge of the center of tuna caudal fins also has a characteristic shape with a notch in the center. This notch is supported by three spatulate and shortened fin rays in the center of the caudal fin.

The large lateral keels occur at the end and narrowest part of the caudal peduncle. Our images show that they have a triangular cross section and are made of collagen (supplementary material; figure 3(b)) and on fresh tissue the keels are soft and rubbery in texture and are remarkably deformable. These fleshy keels also dry out quickly compared to other tissues and because of this, their shape seems to be affected by freezing and formalin fixation. Therefore, our images of fixed tissue still represent the general shape of the keels, but caution should be exercised before using unmodified keel models (supplementary models) in any physical platform—we would recommend 3D scanning of fresh tuna material or modifying our models to correct the warping and curling caused by preservation. The bones of the peduncle region also extend laterally into a bony keel, where the lateral apophyses of the vertebrae (lateral bony projections) are modified into lateral, sheetlike projections (figure 3(a); supplementary models). However, the widest part of the bony keel does not align with the widest part of the fleshy keel—instead the widest part of the bony keel is shifted anteriorly compared to the fleshy keel in both tuna species examined (figure 3; supplementary movies). The neural and haemal spines of the vertebrae (dorsal and ventral bony projections) at the caudal peduncle are also flattened and overlap considerably with the posterior neighboring vertebrae (supplementary models; figure 3) and prevent bending in the dorso-ventral plane.

In the interior of each keel, there is a canal that is filled with a soft matrix of tissue (figure 3; supplementary movies). This canal has branches to the exterior of the lateral keel that open to the outside on the dorsal and ventral surfaces of the keel. This canal is a continuation of the lateral line canal (determined by examining a series of μ CT slices through the keel; also see the supplementary movies), which is a sensory system that fishes use to detect flow and changes in flow. The branches and pores to the external fluid suggest that the embedded lateral line in the keel is sensing flow conditions on the surface of the keel, even though histological sections show that the canal appears to be filled with a soft-tissue matrix (figure 3(d)).

Tuna finlets occur on the dorsal and ventral midline of the body, posterior to the second dorsal and anal fin. They are supported by internal bony pterygiophores, and each finlet has an anterior head that is embedded below the body surface. This finlet head connects to three pairs of muscles and is also where all the fin rays originate (see supplementary models and movies). The fin rays of the finlet do not appear to branch, and the finlet leading edge appears to be composed of many fused fin rays. The fin ray running along the base of each finlet is enlarged relative to the other rays in the finlet. The base of each finlet also has a collar made of small, elongate scales (figure 5; and supplementary figure 1). In mackerel, we observed that finlets are also attached along part of their base with a thin delicate membrane that stretches between the fin rays of the finlet and the body, likely providing enhanced surface area when finlets are abducted away from the body (supplementary figure 1).

Pectoral fins of yellowfin and Pacific bluefin tuna have large, robust fin rays (figure 5). Paired fin rays are significantly asymmetrical, with the medial hemitrich (on the dorsal fin surface when fins are deployed) having a smaller cross section compared to the lateral hemitrich (on the ventral fin surface when fins are deployed). Hemitrichia are also modified compared to most fish fin rays in having hollow cross-sectional shapes at the base. The base of the pectoral fins attaches in a curved fashion to the body so that the trailing edge of the fin is curved ventrally compared to the leading edge (figure 5; supplementary model). This curvature is stronger in Pacific bluefin tuna, which has pectoral fins with a proportionally shorter span and a larger chord compared to yellowfin tuna.

3.2. Locomotor behavior of tunas

We filmed both routine swimming and feeding behaviors of captive live yellowfin tuna to observe their swimming behavior. We estimate that routine swimming speeds were approximately 1 body length per second (~1–1.2 m s⁻¹). Below we describe behaviors involving the finlets and the pectoral fins, both of which exhibit movements reflecting active muscular control.

Finlets rotate about their base at the leading edges and generally mimic the motion of the caudal fin but with a phase difference (figure 6, supplementary movies). More upstream finlets rotate through a smaller angular range than downstream finlets, likely because the more posterior tuna body regions undergo greater lateral excursion and are therefore subject to greater lateral forces during swimming. There is no clear evidence that finlets are actively moved during routine steady swimming because they exhibit motion as expected based on the gradient of hydrodynamic forces (also seen and suggested in mackerels [22, 23]). However, each finlet is connected to three pairs of muscles (see supplementary movies), and we observed instances where finlets are clearly actively moved: (1) during glides where the finlets are actively rotated at an angle and (2) when the last finlet is independently rotated compared to the others (see supplementary movies). In both cases, movement of finlets in a direction against incident hydrodynamic flow provides direct evidence of active control of finlet motion.

Tuna pectoral fins are often deployed laterally, in a manner similar to airplane wings with an adjustable sweep angle, and they can also be held against the body where they fit against grooves made by enlarged, fat-filled scales [38]. One other behavior we witnessed during routine swimming is the deployment or partial deployment of just one pectoral fin (figure 6). In some cases, tunas would swim tens of meters with just one pectoral fin partially or fully deployed, while the other was held against the body.

During feeding sequences, tunas move at much higher speeds and often rapidly change directions. In these situations, the pectoral fins change sweep angle and angle of attack, and complex twisting fin conformations are evident in some maneuvers. In figure 6 we show images from one sequence of a tuna approaching the surface to catch a food item, capturing the food, and then descending away from the surface and turning to avoid the wall. During this maneuver, the pectoral fins substantially change their angle of attack, and contribute to pitching and braking maneuvers for the fish (figure 6). We observed high angles of attack of pectoral fins (approaching 45°) and noted considerable flexibility of the fin surface, which often showed wave-like spanwise twisting movements as a result of rotation at the base.

3.3. Experiments: lateral keels

We tested simple physical models of tuna lateral keels (figure 7) to evaluate the ability of keels to alter swimming performance by reducing lateral forces and yaw torques as a result of altering the lateral profile of the peduncle. Reducing drag forces that result from relatively high amplitude lateral motion in the peduncular (pre-caudal fin) area should reduce the power requirements of swimming. We recorded swimming performance metrics over three speeds with a single motion program using three foils—a biomimetic triangular-keeled foil, a square-keeled foil, and a flat foil (figure 7). These three flow speeds represent conditions where the foils are accelerating (0.3 m s⁻¹ flow speed, net thrust production), station holding $(0.46 \text{ m s}^{-1} \text{ flow speed, zero net thrust})$, and decelerating (negative acceleration; 0.6 m s⁻¹ flow speed, net drag production). We interpret foil conditions as accelerating, station-holding, and decelerating based on the net forces produced in the drag-thrust axis and therefore how the foils would behave in untethered circumstances. We found that the mechanical power required to move the foil is lower in the triangular-keeled foil compared to the other two configurations (TukeyHSD: $p \ll 0.05$, figure 8), however, the triangular keeled foil also generates less thrust (although at the higher flow speed, the triangular and square keeled foils are indistinguishable in thrust generated; TukeyHSD: p < 0.05 at 0.3 and $0.46 \,\mathrm{m\,s^{-1}}$, but p > 0.05 between triangular and square keels at $0.6 \,\mathrm{m \, s^{-1}}$, figure 8).

The lower required power for the triangular keels is mirrored by lower values of yaw torque amplitude during swimming (figure 8; TukeyHSD across speeds: $p \ll 0.05$). Results for lateral force amplitude are not as clearcut; the flat, no-keel foil always generates a lower lateral force amplitude than square keeled foil

(TukeyHSD across speeds p < 0.05), but the triangular keeled foil generates lower lateral force amplitude than the square keeled foil at the $0.3~{\rm m\,s^{-1}}$ speed (TukeyHSD p < 0.05). At the other two swimming speeds the triangular keel is not distinguishable from the square keeled foil (TukeyHSD triangular versus square at $0.46~{\rm and}~0.6~{\rm m~s^{-1}}$: p > 0.05, figure 8). Additional force and torque amplitudes for keel comparisons are shown in the supplementary material (supplementary figure 2).

3.4. Experiments: finlets

Do simple finlet models contribute to thrust generation and reduced power consumption during locomotion? We recorded swimming performance over nine flow speeds (0.35–0.75 m s⁻¹ at 0.05 m s⁻¹ increments) using a single motion program and compared three foils—a biomimetic foil with passively flexible finlets that were attached with a small base, a foil with stiff finlets attached along their entire length, and a foil with long strip fins of the same area as the finlets on its dorsal and ventral edge (figure 7). Power requirements during locomotion were lower for the flexible finlets than for either of the other two finlet foils (TukeyHSD, $p \ll 0.05$, figure 9), and this was accompanied by lower thrust produced by the flexible finlets compared to the other two foils (TukeyHSD, p < 0.05, figure 9).

Flexible finlets generate lower lateral force amplitudes compared to stiff finlets and strip fins at all but the highest tested flow speeds (TukeyHSD, 0.35- 0.7 m s^{-1} : p < 0.05, figure 9). Flexible finlets also have a lower torque amplitude at low flow speeds (0.35-0.45 m s⁻¹), but torque amplitudes are indistinguishable from the stiff finlet foil until the highest swim speed, where again the flexible finlets have lower yaw torque amplitude than the stiff foil (TukeyHSD flexible and stiff at 0.75 m s⁻¹, p < 0.05, figure 9). The strip fin foil is indistinguishable in yaw torque amplitude from the stiff finlet foils until it reaches higher flow speeds $(0.6-0.75 \text{ m s}^{-1})$ where it then has a lower yaw torque amplitude compared to the stiff finlet model (TukeyHSD for stiff and strip fin models at 0.6- 0.75 m s^{-1} , p < 0.05). Additional force and torque amplitude data are included in the supplementary material (supplementary figure 3).

3.5. Experiments: pectoral fin function

We investigated how pectoral fin conformation changes swimming and maneuvering performance using simple physical models. By examining the forces and torques generated by a single pectoral fin model, we also studied how having one deployed fin can generate forces and torques on the body of a tuna. We recorded force and torque data for three different static models across two flow speeds (0.22 m s $^{-1}$ and 0.44 m s $^{-1}$) and three angles of attack (0°, 15°, and 30°). Our three models included: (1) a biomimetic pectoral fin model with a curved pectoral fin base that is attached at both the leading and trailing sides of the model, (2) a pectoral model with a curved base that is only attached

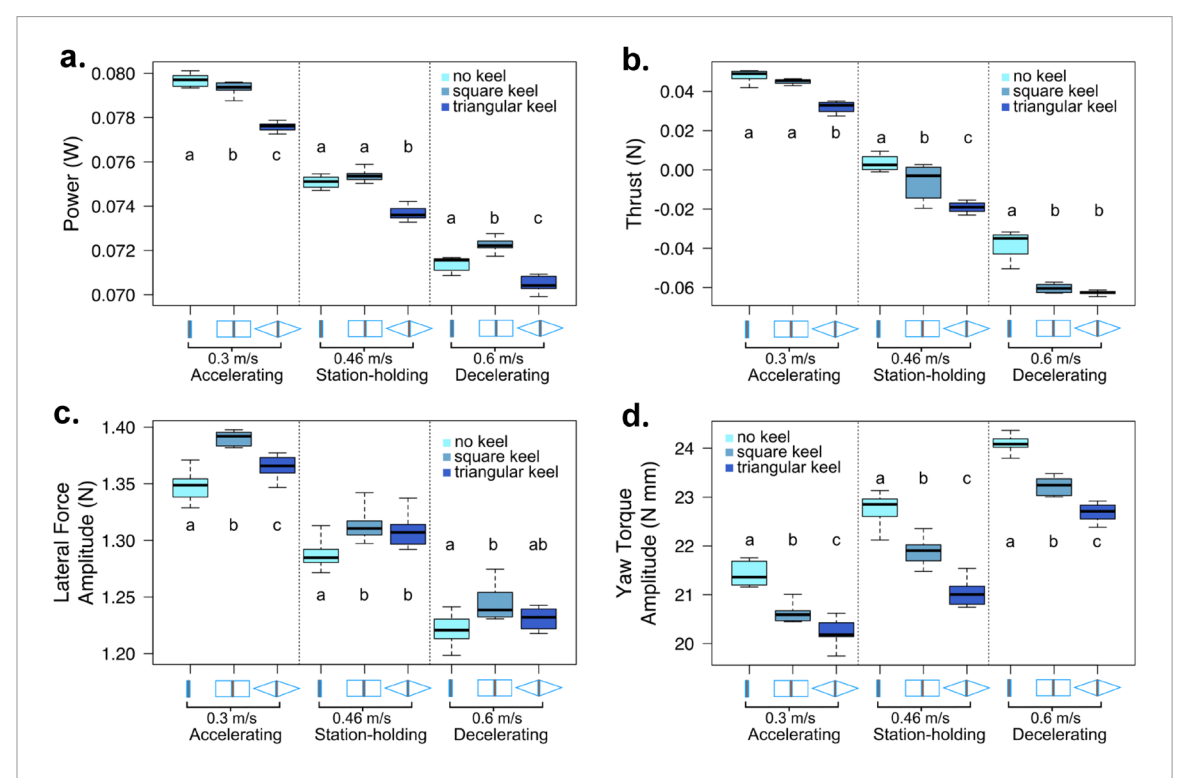


Figure 8. Keel model performance data using the same motion program $(2 \text{ Hz}, \pm 2 \text{ cm heave}, 15\,^{\circ} \text{ pitch}, 90\,^{\circ} \text{ offset between heave}$ and pitch) across different flow speeds. Lowercase letters on graphs indicate significant differences at an alpha level of 0.05 using a TukeyHSD post hoc test after a significant ANOVA result. (a) Mechanical power required to move each model at different flow speeds. (b) Thrust generated. (c) Amplitude of lateral force. (d) Amplitude of yaw torque.

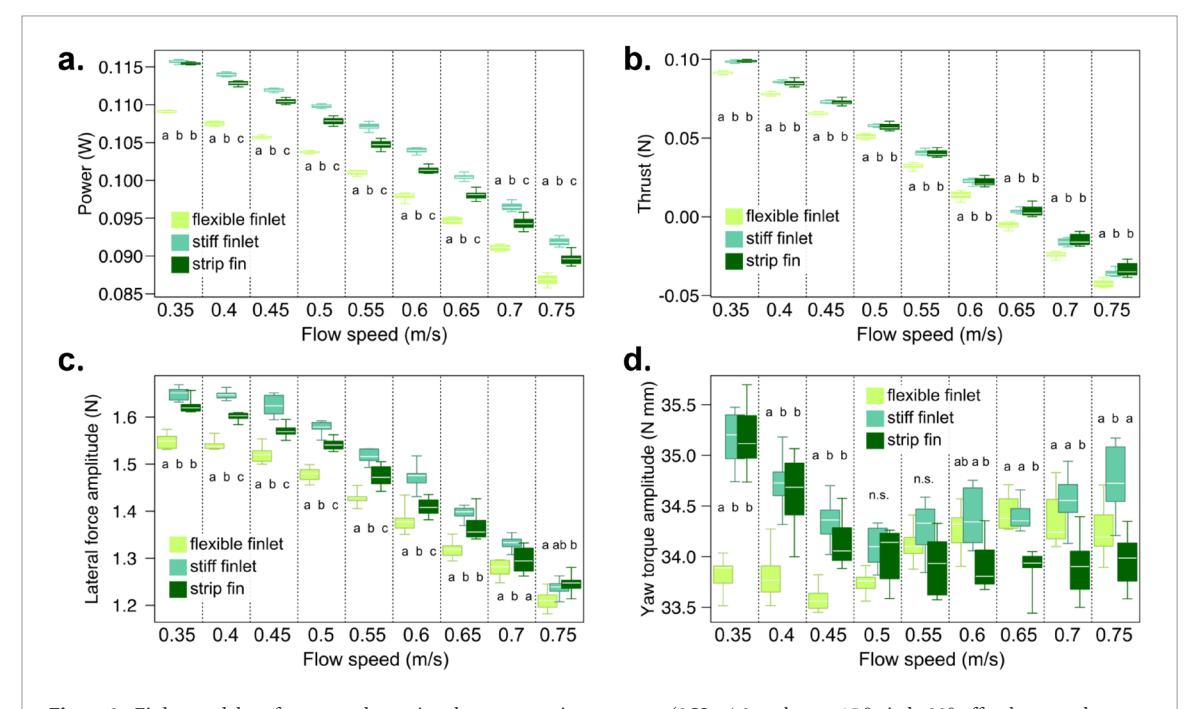


Figure 9. Finlet model performance data using the same motion program $(2 \text{ Hz}, \pm 2 \text{ cm heave}, 15\,^{\circ} \text{ pitch}, 90^{\circ} \text{ offset between heave}$ and pitch) across different flow speeds. Lowercase letters on graphs indicate significant differences at an alpha level of 0.05 using a TukeyHSD post hoc test after a significant ANOVA result. (a) Mechanical power required for movement across speeds. (b) Thrust generated. (c) Amplitude of lateral force. (d) Amplitude of yaw torque.

at the leading side of the model, and (3) a pectoral model that is flat.

The lift to drag ratio data show that the curved pectoral fin model outperforms the flat foil at 0° angle of attack (figure 10; TukeyHSD p < 0.05) and that the biomimetic pectoral fin with both a curved base and fully attached base has a higher lift to drag ratio than

other foils at 0° angle of attack (TukeyHSD p < 0.05). The higher lift to drag of the biomimetic pectoral model can be attributed to higher lift generated by this foil at 0° angles of attack (TukeyHSD $p \ll 0.05$, despite the higher drag of this model across all testing conditions (TukeyHSD p < 0.05). For lateral force and all three torque axes, the biomimetic model with

a curved, fully attached base generates higher forces or torques across all experimental conditions (TukeyHSD p < 0.05).

4. Discussion

The aim of this paper is to provide descriptions and new experimental data relevant to tuna locomotion to better connect research on the biomechanics of highperformance fish swimming with future bioinspired autonomous underwater vehicle (AUV) designs. By studying the morphology, behavior, and performance effects of three different features of high-performance fishes, we can better understand the benefits and tradeoffs of incorporating tuna-inspired caudal keels, finlets, and pectoral fins into future tuna-inspired AUVs. For example, the most recent robotic platform based on tuna includes a caudal keel, but not pectoral fins or finlets [9]. Our goal is to provide a resource for AUV designers interested in high-performance fish morphology, as well as guide AUV design by exploring the potential performance benefits and detriments of utilizing traits shared by tunas and other highperformance fishes. The use of 3D imaging (μ CT) and quantitative performance testing of models has allowed for the discovery of several undescribed features and effects of tuna morphology, and the resulting 3D models can be easily incorporated into future prototype fabrication.

4.1. Tuna body and tail morphology

Tuna have streamlined bodies, but unlike many other high-performance fishes with narrow body shapes, tunas have exceptionally wide bodies as well as small caudal fins for their body size (figure 1). Although previous work has claimed that the tuna body shape has minimal drag [17], caution should be exercised before claiming that tuna body shape is optimal for AUV design (although it does provide considerable space for payloads and actuators). In particular, the endothermic nature of tuna body musculature may explain the wide tuna body shape, as increases in body thickness allow for increased red muscle fiber mass and the counter-current exchange system that helps increase swimming performance by maintaining elevated temperatures in the heat-producing red muscles of tuna [39, 40]. The relationships between body shape, thermal regulation, and drag still remain to be quantified, and the biomechanical effects of a tuna-like body shape on swimming performance remains unstudied (especially compared to other possible body shapes).

Tuna caudal fins are lunate in shape, have robust peduncle vertebrae, and have thickened fin rays that create an airfoil-like cross section along the upper and lower caudal fin lobes (figure 2). The modified neural and haemal spines that overlap with the next posterior vertebrae prevent dorso-ventral bending of the peduncle and permit almost exclusively lateral bending at the

peduncle [19]. Tuna also have two smaller lateral keels near the center of the caudal fin. These smaller keels occur just dorsal and ventral to the larger peduncle keel and are angled towards each other and the center of the fin. Larger but very similar features also occur on marlins, representing a convergent feature in need of functional study. The trailing edge of the center of the caudal fin also has a notched shape that appears to be common to most tuna species. The effect of these smaller features of tuna caudal-fin design are as yet unknown, but together the shape of the caudal fin trailing edge and the small caudal fin keels may subtly affect flows at the center of the fin.

4.2. Morphology and function of tuna lateral keels

The collagenous lateral keels at the peduncle of tunas contain a soft-tissue filled lateral line canal with branches to the skin's surface (figure 3 and supplementary movie). This previously undescribed canal represents a unique modification of the lateral line system and occurs in a potentially important location for flow sensing related to swimming-it would be valuable to investigate the possible presence and locations of neuromasts (groups of cells that sense flow) in the canal in future work. Tunas also have a bony keel made from lateral projections of the peduncle vertebrae, although, surprisingly, this bony keel is offset anteriorly from the collagenous flexible lateral keels and is anatomically distinct from the flexible lateral external keels (figure 3). This offset may reflect a functional difference between bony and collagenous keels, as bony keels are thought to increase the angle of tendon attachment to the caudal fin [21], resulting in larger forces being produced during swimming. In contrast, the collagenous keels are highly flexible and may serve a sensory function in addition to possibly redirecting flow along the mid-tail surface and reducing the effect of posterior yaw torques on side-toside oscillation of the center of mass.

We tested physical models of lateral keels of different cross-sectional shape and found that biomimetic triangular keels required less input power during locomotion, due in part to lower yaw torque amplitudes and somewhat lower lateral force amplitudes when compared to some or all non-biomimetic models (figure 8). Force and yaw torque in the lateral plane are perpendicular to thrust, and thus minimizing these forces and torques likely helps minimize energy input into the swimming platform. We also found that the biomimetic triangular models generate less thrust compared to square-keeled or flat-sided models. Having a large keel on a flat oscillating foil reduces the lateral area for thrust generation (although the squarekeeled foils also generate lower thrust at higher speeds) and it may stiffen the peduncle. It seems likely, however, that thrust generation in tuna by the peduncular surface is low relative to the thrust produced at the caudal fin [19, 23, 35]. Reduced thrust produced by the triangular keels may represent a tradeoff required to

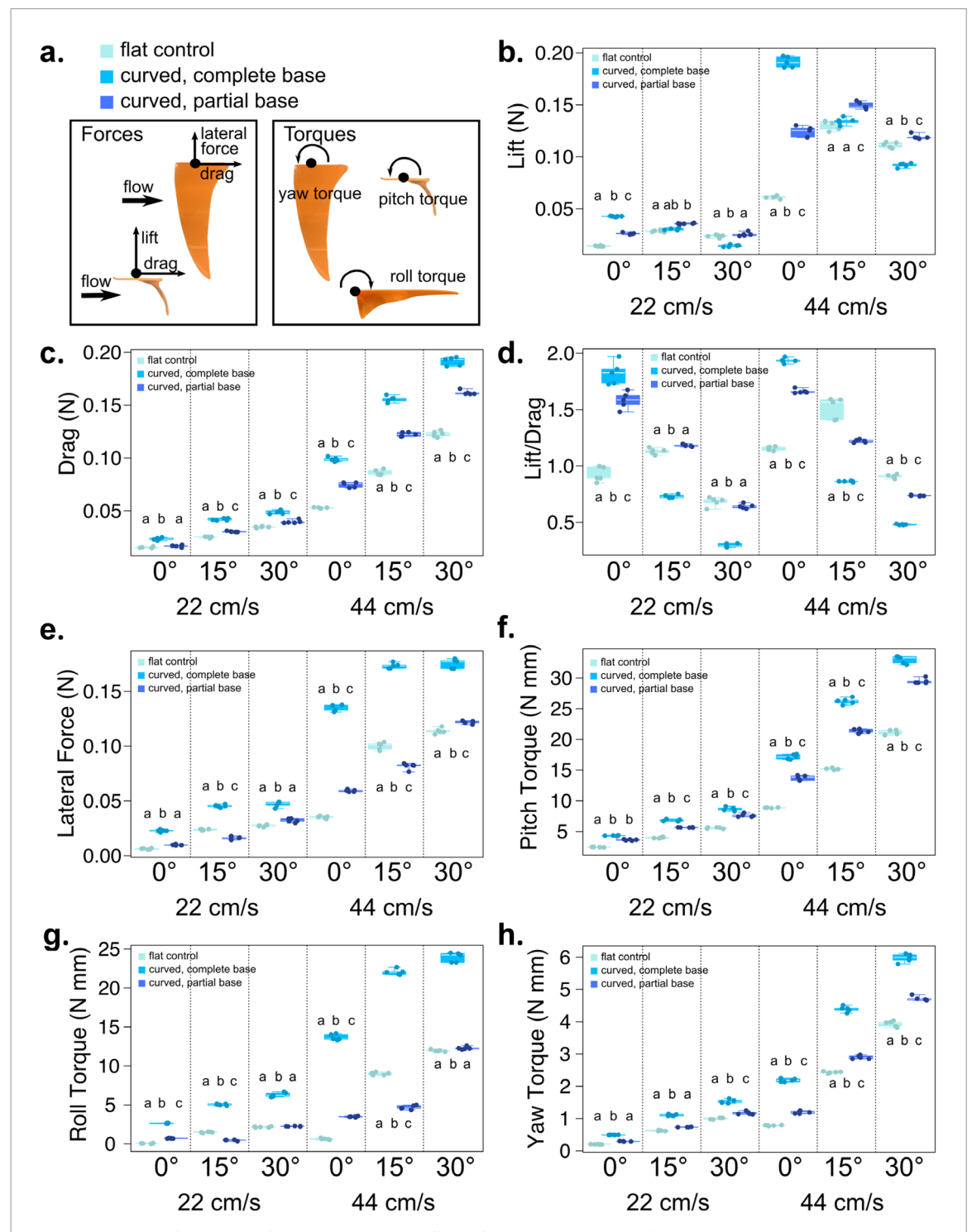


Figure 10. Pectoral fin model performance data across different flow speeds and angles of attack. Lowercase letters on graphs indicate significant differences at an alpha level of 0.05 using a TukeyHSD post hoc test after a significant ANOVA result. All forces are mean force (not amplitude of forces as above) (a) legend for colors and images of model designating the direction of all forces and torques. (b) Lift forces. (c) Drag forces. (d) Lift-to-drag ratio. (e) Lateral force. (f) Pitching torque. (g) Roll torque. (h) Yaw torque.

reduce lateral forces, which in turn may reduce recoil experienced by the anterior body region as a consequence of caudal fin oscillation and thereby generate an increase in overall swimming efficiency.

Previous ideas about the function of tuna lateral keels include laterally streamlining the peduncle during swimming [8, 18], generating lift [24], and organizing flow to increase performance [41]. Our results strongly support the idea that the keeled tuna pedun-

cle assists in laterally streamlining this region, and thereby reduces both forces that do not contribute to thrust and torques produced by oscillating the caudal fin. These reduced forces and torques result in reduced power consumption, but they also may lower thrust production, at least in these simply designed models. Our results do not address the possible role of the keel in lift generation, as our models are open at both the anterior and posterior faces, and both square and

triangular keeled foils have larger lifting force amplitudes than the flat model. However, the external keel is highly flexible, and we suggest that lift generation by this structure is unlikely to be significant given the relatively large forces produced by tuna caudal and pectoral fins during swimming. Overall, these conclusions suggest that keeled peduncles, even simply implemented, may help reduce locomotor costs for any AUV using fish-like undulatory or oscillatory propulsion.

4.3. Function of tuna finlets

Although the external morphology of tuna finlets is generally well known, data on their internal attachments, both muscular and skeletal, is not well documented. Here we provide 3D information on finlet osteology and musculature as well as 3D models for easy fabrication and further study of tuna finlet shape. The leading edge of finlets is composed of an enlarged group of fused fin rays, perhaps to stiffen the leading edge against damage or hydrodynamic forces. As previously documented in mackerel [22, 23], finlets appear to mostly oscillate in a passive manner during steady swimming. However, we also present evidence of clear active use of finlets during glides to change heading. Finally, we also show that mackerel finlets have a clear membrane attaching the medial edge of the finlet to the body (photographs in supplementary material), which should greatly increase effective finlet surface area when it is abducted away from the body (which appears to occur during mackerel locomotion). However, it is unclear if tunas have a similar finlet membrane; we were unable to locate any literature reports on these membranes in tunas, and we did not observe one in our specimens although the membranes are extremely fragile in mackerel and could easily be destroyed when tuna are caught.

We tested simple models of flexible finlets against stiff finlets or strip-shaped fin models of the same total surface area and found that flexible finlet models consume less power compared to stiff finlet and strip finlet models. The reduced power consumption can be explained in part by reduced lateral force amplitudes generated by flexible finlets across all experimental conditions, and smaller yaw torque amplitudes generated at lower flow speeds (0.35–0.45 m s⁻¹; yaw torque is intermediate at higher speeds). Although power consumption is lower, biomimetic, flexible-finlet models also generate less thrust.

These results mirror those of the keeled models—like peduncle keels, finlets are not thrust-producing structures, but they do reduce power consumption in part by also reducing lateral forces. These experimental conclusions support many of the potential hypotheses concerning finlet function, but also do not support the hypothesis that finlets increase thrust. Combined with our behavioral observations and previous studies on the function of finlets or finlet-like structures, we favor the idea that finlets act as flow-fences and help to prevent and redirect cross flow, thus reducing drag.

Additional functional work is needed, perhaps with more complex 3D models combined with computational fluid dynamics, to fully explore the idea of finlets as flow-fences and determine potential performance effects. We also suggest that tuna finlets provide the ability to slowly change heading without modifying body kinematics or even without moving the rest of the body, in a similar manner to previous results from mackerel [22, 23]. Tuna that show active alteration in finlet angle during glides or swimming with a single pectoral fin deployed are evidence that tunas exhibit multiple behaviors that create slow, but presumably low-energy-cost maneuvers. These kinds of behaviors are neither well documented nor well-studied in fishes, although they may be of particular significance in the open ocean environment, which provides effectively unlimited room for maneuvers. Maneuvering in this way may reduce overall energy consumption or perhaps generate diminished hydrodynamic or acoustic signals.

4.4. Morphology and function of tuna pectoral fins

Tuna pectoral fins are reminiscent of swept back wings on aircraft and indeed other authors have implicated tuna pectoral fins in lift force generation, especially at slow swimming speeds [19, 24]. Tuna are negatively buoyant [19, 42], and pectoral and caudal fin lift generation has been proposed to provide counteracting vertical forces and allow steady horizontal locomotion. We note that the hemitrichia (each half of fin rays, see [43, 44]) of the tuna pectoral fin show substantial asymmetry, perhaps indicating asymmetric resistance to forces encountered by these fins during swimming. In addition, the bases of tuna pectoral fins are curved so that the trailing edges curve ventrally (figure 5). Tunas normally swim with either both pectoral fins deployed or both fins abducted against the body, but we also documented tuna swimming with a single pectoral fin either fully or partially deployed. We suggest that this posture may be useful in executing slow maneuvers without changing midline kinematics. We also show the surprisingly dynamic nature of the pectoral fin during high-speed maneuvers. Ostensibly rigid pectoral fins can be deployed at extreme angles of attack to facilitate ascent, descent, and other turning maneuvers, and exhibit complex longitudinal twisting and conformational alterations (figure 6(c)). Clearly tuna pectoral fins are not the static structures that steady swimming behaviors would indicate.

We tested three simple pectoral fin models to explore the effect of having a curved and fully-attached base. Our results show that at 0° angle of attack, the model with a curved and fully-attached base has the best lift-to-drag ratio, largely due to much higher lift produced by this model. At higher angles of attack, having a fully-attached and curved base results in the poorest lift-to-drag performance; however, this model also creates the highest drag, lateral force, pitch torque, roll torque, and yaw torque magnitudes across both

speeds tested (simulating 1 and 2 body-lengths per second) and at all three angles of attack.

These results indicate that having a fully attached and curved pectoral fin gives increased gliding performance at low angles of attack, but also provides the highest capability for maneuvering through torque generation across a range of speeds and angles of attack. The one drawback of this design is that it incurs the greatest drag across testing conditions. Tunas avoid this performance degradation by retracting the pectoral fins when steady-swimming at higher speeds. For biomimetic AUV systems, pectoral fin designs that allow modulation of lift forces as well as torques would certainly be beneficial for controlling pitch and yaw dynamics. Pectoral fins in many fish biorobotic systems tend to have rigid airfoil-like designs to minimize drag when deployed at a zero angle of attack. But our results suggest that, despite the added manufacturing complexity, using complexly curved tuna-like pectoral fin design will enhance lift production and hence pitch responsiveness, and produce increased yaw torques for improved maneuvering performance. In addition, designs that mimic the ability of tuna to retract the fins against the body wall will also reduce drag during steady rectilinear swimming, although such designs also add manufacturing and control complexity.

4.5. How efficient is tuna locomotion?

Tuna are high-performance pelagic fishes capable of both impressive long-distance migrations and rapid local maneuvers during behaviors such as feeding [6, 8, 45–47]. Researchers working in the area of aquatic propulsion often assume that tunas are highly efficient swimmers as a result of their active lifestyle in the open ocean. Efficiency of fish propulsion is most often quantified by measuring the cost of transport, equivalent to energy consumed per unit distance traveled (J m⁻¹) or normalized by mass as energy per kilogram distance, or J $(kg*m)^{-1}$ [48–50]. By these metrics, and compared to many other fishes, tunas are not efficient swimmers, and in fact have a higher cost of transport than most other fish species. Tuna are best thought of as equivalent to a high-performance sports car which is capable of both high acceleration and high sustained speeds but is not the most efficient vehicle in terms of miles per gallon energy consumption.

There are several lines of evidence indicating that tuna have more costly locomotion than other fishes. First, since obtaining cost of transport data on large pelagic fishes such as tuna can be challenging, one metric that is often used as a proxy for energy expenditure and the cost of locomotion is tail beat frequency which is easier to measure. A higher tail beat frequency for a fish species swimming at the same speed as other species is indirect evidence of higher energy costs. Dewar and Graham (1994a: [51]) present kinematic data on swimming fishes including tuna, and tuna have a higher tail beat frequency than other species for swimming speeds lower than about 100 cm s⁻¹. Donley and

Dickson (2000: [52]) conducted a detailed comparison between the kinematics of swimming in kawakawa tuna (*Euthynnus affinis*) and chub mackerel (*Scomber japonicus*) of the same body size, and also found that at the same swimming speed tuna 'displayed a significantly greater tailbeat frequency, but lower stride length, tailbeat amplitude and propulsive wavelength, than chub mackerel when size effects were accounted for'.

Second, cost of transport versus speed plots for fishes typically have a U-shaped profile with a minimum cost at a low to medium swimming speed, and we can examine the cost of transport at this minimum among a diversity of fishes to assess the relative efficiency of tuna. Sepulveda and Dickson (2000: [49]) present metabolic data on mackerel and kawakawa tuna, and these authors present the best available size-matched quantitative comparative data between tuna and mackerel (a tuna relative with a similar body shape). Sepulveda and Dickson (2000, p 3089: [49]) state that 'The juvenile kawakawa had significantly higher standard metabolic rates than the chub mackerel, because the total rate of oxygen consumption at a given swimming speed was higher in the kawakawa when the effects of fish size were accounted for'.

Third, another possible metric that could represent efficient swimming is the slope of the upper limb of the cost of transport versus speed curve. If tuna are highly efficient, then metabolic data should show that tuna possess a lower rate of increase of swimming costs compared to other fishes as speed increases. Dewar and Graham (1994b: [51]) provide metabolic data relevant to this issue. Dewar and Graham (1994b: [51]) show that tuna do in fact have a reduced slope of the oxygen consumption versus swimming speed graph, but this lower slope for tuna is not sufficient to overcome the substantially higher basal metabolic costs. Even with this lower slope, swimming at 125 cm s⁻¹ still leaves salmon (Oncorhynchus nerka) with a lower cost of transport despite being larger than the 1.1 Kg Thunnus albacares specimen used for comparison.

The low-cost energetic champion fish are swimming eels (*Anguilla*) which migrate for thousands of kilometers [53–55]. Due to specialization in metabolic processes related to fat utilization, eels are able to swim with the lowest measured energetic cost of transport for any fish [54].

Fourth, the active pelagic lifestyle of tuna is supported by a large mass of red muscle and internal body temperatures that are warmer than ambient water [40, 56–59]. Elevated body temperatures in tuna have been proposed to extend their thermal niche and allow an active predatory lifestyle in colder waters where prey are unable to be as active with their colder locomotor musculature [8, 59]. Furthermore, warming the internal organs in tuna improves digestive efficiency and permits an increased extraction rate of energy from ingested food. This increased metabolic activity that supports warmer body temperatures comes at a

cost: a higher basal metabolic rate, and this cost must be added to the hydrodynamic and mechanical costs associated with locomotion.

These factors all argue for a view of tuna as highperformance swimming machines, but not with a locomotor system that is more efficient than other fish species.

5. Conclusion

High-performance fishes, such as tunas, are both a performance benchmark and an inspiration for the next generation of autonomous underwater vehicles (AUVs). To help identify and understand features of high-performance fishes that may aid in the development of AUVs, we undertook an investigation of the morphology and behavior of tunas, and then added performance testing of three features of tunas and other high-performance fishes. We quantified tuna morphology in three dimensions to provide the data needed to incorporate a tuna-like body shape, caudal-fin structure, axial skeleton, caudal keels, finlets, or pectoral fins into future biorobotic AUV platforms. Tunas show a great diversity of locomotor behaviors and we particularly describe tunas rapidly maneuvering during feeding, swimming with a single deployed pectoral fin, and actively using their finlets during glides. During periods of rapid acceleration and maneuvering as observed during feeding, pectoral fin conformation changes dramatically, and we observed considerable longitudinal twisting of the pectoral fin. The curved and fully attached base of tuna pectoral fins increases the lift-to-drag ratio at zero angle of attack, and also increases performance at higher attack angles by stabilizing the fin through attachment to the body. Tuna pectoral fin models also generate high torques that should enhance maneuvers. Caudal keels and finlets do not provide additional thrust but can reduce power requirements of swimming under certain motion programs, and we observe active control of finlets during low-speed maneuvers. Tunas remain a source of inspiration for designing future AUVs, and a wealth of untapped biological information on tunas likely remains to be discovered and applied to future engineering designs.

Acknowledgments

This work was supported in part by the Office of Naval Research MURI Grant N000141410533 to GVL, monitored by Bob Brizzolara, and NSF GRF DGE-1144152 and PRF-1907156 to DKW. We are very grateful to Prof Terry Bradley (Univ. of Rhode Island) and Peter Mottur (Greenfins, Inc.) for allowing us to film in the Greenfins tuna facility, and to members of the Lauder Lab (Harvard University: Dan Madigan, Terry Dial, Zane Wolf, Dave Matthews, and Valentina Di Santo) for assistance with data acquisition. We also thank William Goldsmith, Prof Diego Bernal (Univ.

of Mass. Dartmouth), and Toby Arakawa (Tropic Fish Hawaii) for help with specimen acquisition.

Data accessibility

We provide lower resolution models and videos associated with this work as part of the supplement, but we also provide full resolution models and videos at https://osf.io/s7mw6/.

ORCID iDs

Dylan K Wainwright https://orcid.org/0000-0003-4964-5048
George V Lauder https://orcid.org/0000-0003-

References

0731-286X

- [1] Du R, Li Z, Youcef-Toumi K and Valdivia y Alvarado P 2015 Robot Fish. Bio-Inspired Fishlike Underwater Robots (Berlin: Springer)
- [2] Long J H, Schumacher J, Livingston N and Kemp M 2006 Four flippers or two? Tetrapodal swimming with an aquatic robot *Bioinspir. Biomim.* 1 20–9
- [3] Liao P, Zhang S and Sun D 2018 A dual caudal-fin miniature robotic fish with an integrated oscillation and jet propulsive mechanism *Bioinspir. Biomim.* 13 036007
- [4] Gravish N and Lauder GV. 2018 Robotics-inspired biology J. Exp. Biol. 221 1–8
- [5] Karakasiliotis K, Thandiackal R, Melo K, Horvat T, Mahabadi N K, Tsitkov S, Cabelguen J M and Ijspeert A J 2016 From cineradiography to biorobots: An approach for designing robots to emulate and study animal locomotion J. R. Soc. Interface 13 20151089
- [6] Madigan D J, Baumann Z, Carlisle A B, Hoen D K, Popp B N, Dewar H, Snodgrass O E, Block B A and Fisher N S 2014 Reconstructing transoceanic migration patterns of Pacific bluefin tuna using a chemical tracer toolbox *Ecology* 95 1674–83
- [7] Block B A, Teo S L H, Walli A, Boustany A, Stokesbury M J W, Farwell C, Weng K C, Dewar H and Williams T D 2005 Electronic tagging and population structure of Atlantic bluefin tuna Nature 434 1121–7
- [8] Graham J B and Dickson K A 2004 Tuna comparative physiology J. Exp. Biol. 207 4015–24
- [9] Zhu J, White C, Wainwright D K, Di Santo V, Lauder G V and Bart-Smith H 2019 Tuna robotics: A high-frequency experimental platform exploring the performance space of swimming fishes Sci. Robot. 4 eaax4615
- [10] Masoomi S F, Gutschmidt S, Chen X Q and Sellier M 2015 The kinematics and dynamics of undulatory motion of a tunamimetic robot Int. J. Adv. Robot. Syst. 12 1–11
- [11] Chen H, Zhu C, Yin X, Xing X and Cheng G 2007 Hydrodynamic analysis and simulation of a swimming bionic robot tuna J. Hydrodyn. 19 412–20
- [12] Anderson J M and Chhabra N K 2002 Maneuvering and stability performance of a robotic tuna *Integr. Comp. Biol.* 42 118–26
- [13] Barrett D S, Triantafyllou M S, Yue D K P, Grosenbaugh M A and Wolfgang M J 1999 Drag reduction in fish-like locomotion J. Fluid Mech. 392 183–212
- [14] Triantafyllou M S, Techet A H, Zhu Q, Beal D N, Hover F S and Yue D K P 2002 Vorticity control in fish-like propulsion and maneuvering *Integr. Comp. Biol.* 42 1026–31
- [15] Kishinouye K 1923 Contributions to the comparative study of the so-called Scombroid fishes J. Coll. Agric. Tokyo Imp. Univ. 8 295–473

- [16] Potthoff T 1975 Development and structure of the caudal complex, the vertebral column, and the pterygiophores in the blackfin tuna (*Thunnus atlanticus*, Pisces, Scombridae) Bull. Mar. Sci. 25 205–31
- [17] Fierstine H L and Walters V 1968 Studies in locomotion and anatomy of scombroid fishes *Mem. South. Calif. Acad. Sci.* **6** 1–31
- [18] Walters V 1962 Body form and swimming performance in Scombroid fishes *Am. Zool.* **2** 143–9
- [19] Magnuson J J 1973 Comparative study of adaptations for continuous swimming and hydrostatic equilibrium of scombroid and xiphoid fishes Fish. Bull. 71 337–56
- [20] Collette B B and Nauen C E 1983 FAO Species Catalogue. Vol 2. Scombrids of the World. An annotated and Illustrated Catalogue of Tunas, Mackerels, Bonitos and Related Species Known to Date FAO Fish. Synop. 125 137
- [21] Westneat M W, Hoese W, Pell C A and Wainwright S A 1993 The horizontal septum: mechanisms of force transfer in locomotion of Scombrid fishes (Scombridae, Perciformes) J. Morphol. 217 183–204
- [22] Nauen J C and Lauder G V 2000 Locomotion in scombrid fishes: morphology and kinematics of the finlets of the chub mackerel (Scomber japonicus) *J. Exp. Biol.* **203** 2247–59
- [23] Nauen J C and Lauder G V 2001 Locomotion in scombrid fishes: visualization of flow around the caudal peduncle and finlets of the chub mackerel Scomber japonicus J. Exp. Biol. 204 2251–63
- [24] Magnuson J J 1970 Hydrostatic equilibrium of *Euthynnus affinis*, a pelagic teleost without a gas bladder *Copeia* 1970 56–85
- [25] Aleev Y G 1969 Function and Gross Morphology in Fish ed H Mills (Jerusalem: Keter Press)
- [26] Helfman G S, Collette B B, Facey D E and Bowen B W 2009 *The Diversity of Fishes* (Hoboken, NJ: Wiley)
- [27] Liu G, Ren Y, Dong H, Akanyeti O, Liao J C and Lauder G V. 2017 Computational analysis of vortex dynamics and performance enhancement due to body-fin and fin-fin interactions in fish-like locomotion *J. Fluid Mech.* 829 65–88
- [28] Wainwright P C, Bellwood D R and Westneat M W 2002 Ecomorphology of locomotion in labrid fishes Environ. Biol. Fishes 65 47–62
- [29] Drucker E G and Lauder G V 1999 Locomotor forces on a swimming fish: three-dimensional vortex wake dynamics quantified using digital particle image velocimetry J. Exp. Biol. 202 2393—412
- [30] Descamps E, Sochacka A, de Kegel B, Van Loo D, Hoorebeke L and Adriaens D 2014 Soft tissue discrimination with contrast agents using micro-CT scanning Belgian J. Zool. 144 20–40
- [31] Gignac P M et al 2016 Diffusible iodine-based contrastenhanced computed tomography (diceCT): an emerging tool for rapid, high-resolution, 3D imaging of metazoan soft tissues *J. Anat.* 228 889–909
- [32] Shelton R M, Thornycroft P J M and Lauder GV 2014 Undulatory locomotion of flexible foils as biomimetic models for understanding fish propulsion J. Exp. Biol. 217 2110–20
- [33] Quinn D B, Lauder G V and Smits A J 2014 Flexible propulsors in ground effect *Bioinspir*. *Biomim*. 9 036008
- [34] Rosic MLN, Thornycroft PJM, Feilich KL, Lucas KN and Lauder GV. 2017 Performance variation due to stiffness in a tuna-inspired flexible foil model *Bioinspir.Biomim.* 12 016011
- [35] Feilich K L and Lauder GV. 2015 Passive mechanical models of fish caudal fins: effects of shape and stiffness on selfpropulsion *Bioinspir.Biomim.* 10 036002
- [36] Lauder G.V., Lim J, Shelton R, Witt C, Anderson E and Tangorra J L 2011 Robotic models for studying undulatory locomotion in fishes Mar. Technol. Soc. J. 45 41–55
- [37] Signal Developers 2013 signal: Signal processing (http://r-forge.r-project.org/projects/signal/)
- [38] Wainwright D K, Ingersoll S and Lauder G V 2018 Scale diversity in bigeye tuna (*Thunnus obesus*): fat-filled trabecular scales made of cellular bone *J. Morphol.* 279 828–40

- [39] Malte H, Larsen C, Musyl M and Brill R 2007 Differential heating and cooling rates in bigeye tuna (*Thunnus obesus* Lowe): a model of non-steady state heat exchange *J. Exp. Biol.* 210 2618–26
- [40] Carey F G and Teal J M 1966 Heat conservation in tuna fish muscle Proc. Natl Acad. Sci. 56 1464–9
- [41] Korsmeyer K E and Dewar H 2001 Tuna metabolism and energetics *Tuna: Physiology, Evology and Evolution* (New York: Academic) pp 35–78
- [42] Bernal D, Sepulveda C, Musyl M and Brill R 2009 The ecophysiology of swimming and movement patterns of tunas, billfishes, and large pelagic sharks Fish Locomotion (Oxford: Oxford University Press) pp 436–83
- [43] Lauder G V 2015 Flexible fins and fin rays as key transformations in ray-finned fishes *Great Transformations in Vertebrate Evolution* ed K P Dial *et al* (Berkeley, CA: University of California Press) pp 31–45
- [44] Flammang B E, Alben S, Madden P G A and Lauder G V. 2013 Functional morphology of the fin rays of teleost fishes J. Morphol. 274 1044–59
- [45] Block B A et al 2011 Tracking apex marine predator movements in a dynamic ocean Nature 475 86–90
- [46] Bernal D, Dickson K A, Shadwick R E and Graham J B 2001 Review: analysis of the evolutionary convergence for high performance swimming in lamnid sharks and tunas Comp. Biochem. Physiol. A 129 695–726
- [47] Graham J B and Dickson K A 2000 The evolution of thunniform locomotion and heat conservation in scombrid fishes: new insights based on the morphology of *Allothunnus* fallai Zool. J. Linn. Soc. 129 419–66
- [48] Di Santo V, Kenaley C P and Lauder G V. 2017 High postural costs and anaerobic metabolism during swimming support the hypothesis of a U-shaped metabolism–speed curve in fishes *Proc. Natl Acad. Sci. USA* 114 13048–53
- [49] Sepulveda C and Dickson K A 2000 Maximum sustainable speeds and cost of swimming in juvenile kawakawa tuna (Euthynnus affinis) and chub mackerel (Scomber japonicus) J. Exp. Biol. 203 3089–101
- [50] Brett J R 1964 The respiratory metabolism and swimming performance of young sockeye salmon *J. Fish. Res. Board Can.*
- [51] Dewar H and Graham J B 1994 Studies of tropical tuna swimming performance in a large water tunnel. I. Energetics J. Exp. Biol. 192 13–31
- [52] Donley J M and Dickson K A 2000 Swimming kinematics of juvenile kawakawa tuna (*Euthynnus affinis*) and chub mackerel (*Scomber japonicus*) J. Exp. Biol. 203 3103–16
- [53] Van Den Thillart G, Van Ginneken V, Körner F, Heijmans R, Van Der Linden R and Gluvers A 2004 Endurance swimming of European eel J. Fish Biol. 65 312–8
- [54] Van Ginneken V, Antonissen E, Müller U K, Booms R, Eding E, Verreth J and Van Den Thillart G 2005 Eel migration to the Sargasso: remarkably high swimming efficiency and low energy costs J. Exp. Biol. 208 1329–35
- [55] Van Ginneken V J T and Van Den Thillart G E E J M 2000 Eel fat stores are enough to reach the Sargasso *Nature*
- [56] Block B A and Finnerty J R 1994 Endothermy in fishes: a phylogenetic analysis of constraints, predispositions, and selection pressures *Environ. Biol. Fishes* 40 283–302
- [57] Dickson K A, Johnson N M, Donley J M, Hoskinson J A, Hansen M W and D'Souza Tessier J 2000 Ontogenetic changes in characteristics required for endothermy in juvenile black skipjack tuna (Euthynnus lineatus) J. Exp. Biol. 203 3077–87
- [58] Block B A and Stevens G 2001 Fish physiology: Tuna: Physiology, Ecology and Evolution vol 19, ed W Hoar et al (New York: Academic)
- [59] Block B A et al 2001 Migratory movements, depth preferences, and thermal biology of Atlantic bluefin tuna Science 293 1310–4